Journal of the European Ceramic Society 41 (2021) 611–616

Contents lists available at ScienceDirect

Journal of the European Ceramic Society

journal homepage: www.elsevier.com/locate/jeurceramsoc

Original article

Heterostructural phase diagram of Ga_2O_3–based solid solution with Al_2O_3

Hyeon Woo Kim [a,b], Hyunseok Ko [a], Yong-Chae Chung [b], Sung Beom Cho [a,*]

[a] Convergence Technology Division, Korea Institute of Ceramic Engineering and Technology (KICET), Jinju-si, Gyeongsangnam-do 52851, Republic of Korea
[b] Division of Materials Science and Engineering, Hanyang University, Seoul, 04763, Republic of Korea

ARTICLE INFO

Keywords:
Ultra-wide bandgap
Solid solution
Ga2O3
Heterostructural alloy
First-principles calculation

ABSTRACT

Ga_2O_3, which is emerging as semiconductor material due to the ultra-wide bandgap, has tunability in bandgap and lattice constant by alloying Al. However, successful control of alloying phase is still challenging due to its heterostructural nature and rich polymorphs. Here, we identified the thermodynamic phase diagram of heterostructural $(Al_xGa_{1-x})_2O_3$ alloy. Using density-functional theory (DFT) calculations and regular solution model, we calculated the Gibbs-free energy of mixing of heterostructural polymorphs. Based on the calculation, we show the phase diagram of $(Al_xGa_{1-x})_2O_3$ alloy system with a markedly increased metastability than the isostructural alloy, which can make a vast phase space for homogeneous single-phase alloys. We also investigated the correlation between the bandgap and lattice constant within these systems using hybrid DFT calculations, which can guide the device design of Ga_2O_3 power electronics.

1. Introduction

As an ultra-wide bandgap semiconductor, Ga_2O_3 is rapidly emerging as a promising candidate for potential electronic applications such as high-power transistors and solar-blind photodetectors [1–7]. Among the diversiform polymorphs of Ga_2O_3 [8–10], β-Ga_2O_3 attracted a lot of attention due to its stable form under general environmental conditions and the availability of high-quality substrates grown by melt-based techniques [11,12]. On the other hand, metastable α-Ga_2O_3 shows the corundum structure, which has better compatibility with Al_2O_3 and other conventional oxide semiconductors [13]. Also, α-Ga_2O_3 has a larger bandgap than those of the different phases, thereby shows better Baliga's Figure of Merits [14]. Another metastable phase, ε-Ga_2O_3, shows ferroelectric properties and is considered to polar engineering [15,16]. The unique physical features of each of these polymorphs are attractive for various device applications.

Another fascinating feature of the Ga_2O_3-based device is its wide-range tunability for the device design, which came from its availability for n-type doping [17] and band engineering by alloying Al [18,19]. The combination of doping and alloying enables the modulation doping, which leads to two-dimensional electron gas (2DEG) and unique functionality. While many of n-type doping strategies are well established [20–22], however, the successful alloying control is difficult yet [23–25]. There are still controversial reports on the solubility and polymorphs in Al_2O_3-Ga_2O_3 solid solution [26–30]. This is because of the lack of understanding of the phase competition in the alloying process. The most stable crystal structures of Ga_2O_3 and Al_2O_3 are the monoclinic and corundum structures, respectively. Because their ground states are very different, the alloying process is always heterostructural. Compared to isostructural alloys, heterostructural alloys can exhibit a markedly increased range of the metastable region for the binodal and spinodal lines, thereby opening up a vast phase space for novel homogeneous alloy engineering [31].

In this article, we have investigated the stability of $(Al_xGa_{1-x})_2O_3$ alloy system as a function of the molar concentration in the disordered corundum and monoclinic structures using first-principles density-functional theory (DFT) calculations combining with the regular solution model. We have also investigated the conditions for spontaneous reaction in a heterostructural $(Al_xGa_{1-x})_2O_3$ alloy system by evaluating the Gibbs-free energy of mixing. Furthermore, using the calculated phase diagram based on evaluated the free energy, we show that $(Al_xGa_{1-x})_2O_3$ alloy system is attractive due to its controllable metastability by the molar concentration and temperature. Also, the heterostructural metastability of $(Al_xGa_{1-x})_2O_3$ alloy system promises broader tunability on the bandgap and lattice constant.

2. Computational methods

DFT calculations were performed using the VASP package [32] and projector augmented-wave potentials [33]. The plane-wave basis set

* Corresponding author.
E-mail address: sb.cho@outlook.com (S.B. Cho).

https://doi.org/10.1016/j.jeurceramsoc.2020.08.067
Received 8 June 2020; Received in revised form 27 August 2020; Accepted 28 August 2020
Available online 1 September 2020

was expanded to cutoff energy of 520 eV to minimize Pulay stress during the structural optimization. The structural optimization was truncated until the Hellmann-Feynman forces were under 0.01 eV/Å. The Brillouin zone was sampled using 100 *k*-points density per inverse Å^3 of reciprocal cell. The 3d, 4s, and 4p states of Ga, 3s and 3p states of Al and 2s and 2p states of O are taken as valence states, and the exchange-correlation energy of valence electrons was described using the Perdew, Burke, and Ernzerhof (PBE) functional [34]. The bandgaps were calculated using the Heyd-Scuseria-Ernzerhof (HSE) hybrid functionals [35] with a mixing parameter of 0.32 to fit the experimental bandgaps of Ga_2O_3 and Al_2O_3, as shown in Table 1. The determined mixing parameter is also adopted to calculate the bandgap of the disordered alloy.

3. Results and discussions

The end member of the solid solution, Ga_2O_3 and Al_2O_3, have very different crystal structure in the ground state; thereby, all the alloying process is heterostructural. The crystal structures of ground states of Ga_2O_3 and Al_2O_3 are monoclinic and corundum structures with the $C2/m$ and $R\bar{3}c$ space groups, respectively. The monoclinic structure of Ga_2O_3 is known as β-Ga_2O_3, and the corundum structure of Al_2O_3 is known as α-Al_2O_3. Interestingly, those crystal structures can be observed as polymorphs of those oxides. The corundum structure of Ga_2O_3 is known as the α-Ga_2O_3 phase, and the monoclinic structure of Al_2O_3 is known as the θ-Al_2O_3 phase. Those structures are the metastable state of Ga_2O_3 and Al_2O_3, respectively. The crystal structures of α-Al_2O_3 for corundum, β-Ga_2O_3 for monoclinic, and $(Al_xGa_{1-x})_2O_3$ alloy systems are shown in Fig. 1. To model $(Al_xGa_{1-x})_2O_3$ random alloy system by special quasirandom structures (SQS) [38], we used the *mcsqs* code of the Alloy Theoretic Automated Toolkit (ATAT) [39]. Also, we matched the lattice constant of the SQS models to perform calculations in the equally sized supercell due to disordered structure and used primitive cells to reduce calculation cost. We found that the 80-atom SQS supercells are enough to obtain the perfect disordered correlation between cation pairs in the corundum and monoclinic structures [39].

To examine the stability of the alloy as a function of the molar concentration, we compared their enthalpy of mixing (ΔH_{mix}) in the monoclinic and corundum structures, defined as:

$$\Delta H_{mix}\left[(Al_xGa_{1-x})_2O_3\right] = E\left[(Al_xGa_{1-x})_2O_3\right] - (1-x)E[Ga_2O_3] - xE[Al_2O_3] \quad (1)$$

where $E\left[(Al_xGa_{1-x})_2O_3\right]$ is the total energy of the SQS supercell structure representing the random alloy, and $E[Ga_2O_3]$ and $E[Al_2O_3]$ are the total energies of the Ga_2O_3 and Al_2O_3 in the ground state. All of these values can be obtained from the DFT[1] calculations. This enthalpy of mixing can be expressed with the regular solution model for heterostructural alloy [40,41] in the form of

$$\Delta H_{mix}(x) = (1-x)\Delta H_0 + x\Delta H_1 + x(1-x)\Omega \quad (2)$$

Table 1
Calculated bandgap of Al_2O_3 and Ga_2O_3 in the monoclinic and corundum structures.

Structure	Oxide	Bandgap (eV)	
		Calc.	Exp.
Corundum	Ga_2O_3	5.26	5.32 [30]
	Al_2O_3	8.78	8.8 [36]
Monoclinic	Ga_2O_3	4.52	4.76 [37]
	Al_2O_3	6.96	

[1] An unexpected end of paragraph

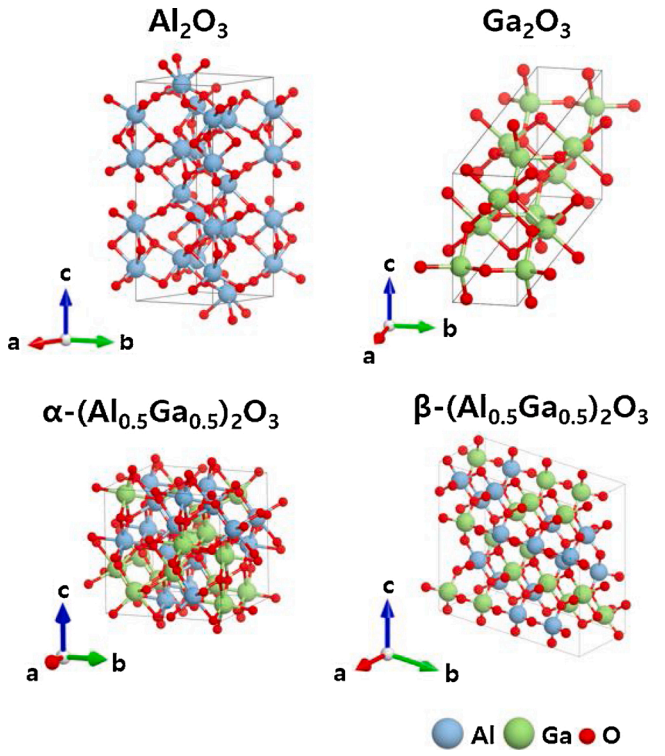

Fig. 1. Atomic structures of Al_2O_3 for corundum, Ga_2O_3 for monoclinic, and $(Al_{0.5}Ga_{0.5})_2O_3$ for both structures. The light blue, light green, and red atoms represent Al, Ga, and O, respectively.

where x is the molar concentration, H_0 and H_1 are the enthalpies of the endpoints for Ga_2O_3 and Al_2O_3, Ω is the regular solution interaction parameters which are the bond energies (U) difference between unequal and equal atomic species $\Omega = 2U_{AlGa} - U_{AlAl} - U_{GaGa}$. If Ω has a negative sign, the mixing is exothermic, which means alloying is always more stable than separated two end members regardless of temperature. On the other hand, the positive Ω value indicates the mixing process is endothermic, which means the stability depends on temperature. We sampled 5 different points of $x = 0$, 0.25, 0.5, 0.75, 1 and evaluated the Ω by fitting the single-parabolic equation eq. (2). The evaluated interaction parameters Ω are shown in Table 2. Based on the evaluated interaction parameters, we found the enthalpy of mixing in $(Al_xGa_{1-x})_2O_3$ alloy system and compared with the ordered structures [18], as shown in Fig. 2.

For the monoclinic structure of pure Ga_2O_3, in which Al was not alloyed ($x = 0$), enthalpy was lower than that of the corundum structure, as shown in the orange line of Fig. 2. This is consistent with the monoclinic of Ga_2O_3 being the stable structure under general environmental conditions [9]. By increasing the Al concentration in the monoclinic alloy structure, the enthalpy of mixing also gradually increases in most of the region, keeping the enthalpy lower than that of the corundum phase. This means the alloy prefers the monoclinic structure. However, when the molar concentration x was 0.84, the enthalpy of mixing of the monoclinic structure was higher than that of the corundum structure. Where the Al concentration is high, the corundum structure

Table 2
Interaction and bowing parameters obtained by fitting enthalpy of mixing and bandgap in $(Al_xGa_{1-x})_2O_3$ alloy system.

Alloy system	Structure	Ω (interaction parameter, meV/f.u.)	*b* (bowing parameter, eV)
$(Al_xGa_{1-x})_2O_3$	Corundum	249	2.13
	Monoclinic	121	−0.32

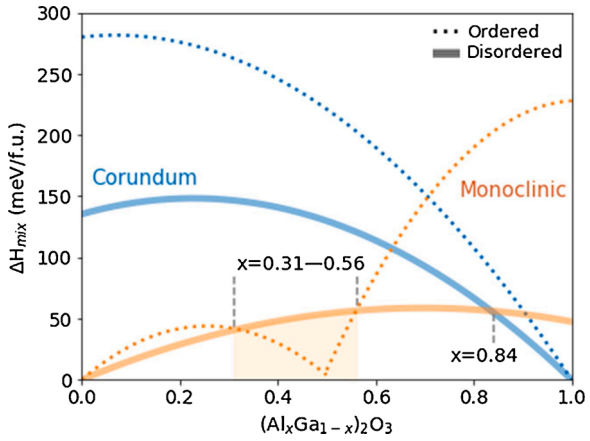

Fig. 2. The comparison of enthalpies of mixing between the ordered [18] and disordered $(Al_xGa_{1-x})_2O_3$ alloy systems in the corundum and monoclinic structures as a function of the molar concentration. The orange and light blue lines represent in the monoclinic and corundum structures, respectively. The shaded region represents the molar concentration range where enthalpy of mixing of the ordered system is lower than that of the disordered system in the monoclinic structure.

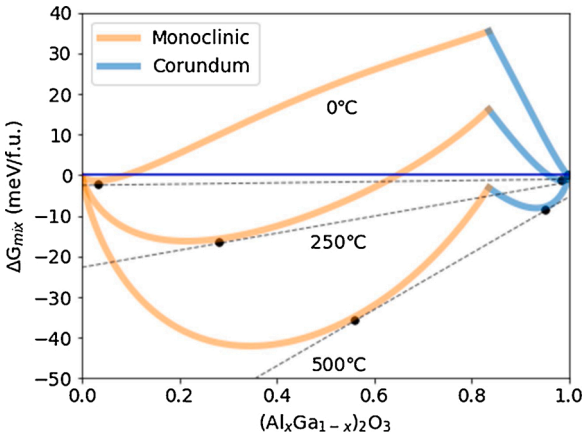

Fig. 3. The effect of temperature on the Gibbs-free energy of mixing of $(Al_xGa_{1-x})_2O_3$ alloy systems, at 0, 250, and 500 ℃. The orange and light blue lines represent for the monoclinic and corundum structures, respectively. The deep blue line is zero value of the Gibbs-free energy of mixing. The common tangent lines and contact points are gray dash lines and black markers.

becomes more favorable.

We find that the disordered monoclinic $(Al_xGa_{1-x})_2O_3$ alloy is more favorable than the corundum structure, consistent with the reported β-phase results [26–28]. Since the cations can be arranged non-randomly, so we also compared the stability of the cation-disordered alloy structure with the ordered structure [18]. The orderly arranged $(Al_xGa_{1-x})_2O_3$ alloy system showed that the corundum structure was preferred over the disordered structure, as shown in Fig. 2. This is because Al prefers to enter the octahedral position over the tetrahedral position [18]. Although the disordered cation distribution is favored in most of the regions in the monoclinic structure, there is a narrow region where ordered alloys are favorable, at the molar concentrations x between 0.31 and 0.56. The value of energy difference is less than approximately 45 meV per formula unit, which can be overcome by the entropy contribution with increasing temperature. We find that the disordered $(Al_xGa_{1-x})_2O_3$ alloy system prefers the monoclinic structure over the corundum structure by comparing enthalpy of mixing as a function of the molar concentration.

Temperature is another crucial criteria for the phase competition. The stability of alloy is determined by the Gibbs-free energy, which includes not only the enthalpy but also the contribution of entropy and temperature. The Gibbs-free energy of mixing is given as follows:

$$\Delta G_{mix}(x,T) = \Delta H_{mix}(x) - T\Delta S_{mix}(x) \tag{3}$$

The Gibbs-free energy has temperature dependency with ΔS_{mix} as shown in Fig. 3. The ΔS_{mix} is the contribution of entropy through the random occupation of ions in the mixing process, which is given by:

$$\Delta S_{mix}(x) = -nk_B[xln(x) + (1-x)ln(1-x)] \tag{4}$$

[3] where k_B is a Boltzmann constant value of 8.617×10^{-5} (eV/K), n is the cation site degeneracy. At 100 ℃, the calculated contribution of the $T\Delta S_{mix}$ term is 45 meV, which is enough to overcome the energy difference in the order/disorder phase. Because most of the alloy deposition process condition has a higher temperature than 100 ℃, hereafter we only considered the disordered structure for the alloys.

To schematize the stability of the alloying process, identifying the phase diagram is required for the design of alloy devices. The phase diagram is determined by calculating the spinodal and binodal lines. The spinodal line is defined by the condition that the second derivative of the Gibbs-free energy of mixing is zero, $\frac{d^2}{dx^2}\Delta G_{mix} = 0$, which classifies the miscibility gap. In the region of $\frac{d^2}{dx^2}\Delta G_{mix} < 0$, even a small fluctuation in the molar concentration leads to a phase separation known as the spinodal decomposition. This is because they are energetically unstable against fluctuation in the local molar concentration. The binodal line is defined by the common tangent of the Gibbs-free energy of mixing. Between the spinodal and binodal lines, the $\frac{d^2}{dx^2}\Delta G_{mix}$ is positive and the alloys are thermodynamically metastable. In this region, once the alloy is formed in a single-phase, it does not decompose spontaneously though it is not under thermal equilibrium. In other words, a novel structure of alloy systems can be obtained in this region [31]. The region above the binodal line is thermodynamically most stable and homogeneous alloy is formed.

We calculated the phase diagram of $(Al_xGa_{1-x})_2O_3$ alloy system to identify structure competition as a function of the molar concentration and temperature during the alloying process. As shown in Fig. 4, the stable/metastable/unstable regions of $(Al_xGa_{1-x})_2O_3$ alloy systems were divided. The stable regions will show the homogeneous single-phase alloys. In the stable state of alloys, the monoclinic structure has a relatively wider homogeneous region than the corundum structure, consistent with the experimental reports synthesized by plasma-assisted molecular beam epitaxy (PAMBE) [26,27] and metalorganic chemical vapor deposition (MOCVD) [28] on the β-Ga_2O_3 substrate. Furthermore, the report of the hydrothermal method [29] without substrate is consistent with our work that both monoclinic and corundum synthesis structures are well alloyed.

Synthesizing the material to the metastable state is another way to make a homogeneous single-phase. The heterostructural alloy is known to have a better thermodynamic solubility limit to metastability than the isostructural alloy [31]. As shown in the white region of Fig. 4, the metastable state of $(Al_xGa_{1-x})_2O_3$ alloy system has a region that can compete for the stable region, consistent with the experimental reports synthesized by the hydrothermal method [29] without the strain effect caused by the substrate. This means that both of $(Al_xGa_{1-x})_2O_3$ alloy phases can be synthesized with metastability in the broad region. We find that the $(Al_xGa_{1-x})_2O_3$ alloy system is easily accessible for metastability than the isostructural alloy, such as $(Al_xGa_{1-x})_2N_3$ [42], and has more rooms to achieve phase engineering using various epitaxial engineering techniques. However, if the effect of epitaxy is considered, the thermodynamic ground state can be overcome. For instance, the mist chemical vapor deposition (MCVD) [30] on the c-plane sapphire substrate, the formation of α-Ga_2O_3 is reported. This is because of the epitaxial interface effect of sapphire substrate and the complex chemistry in MCVD compared to MBE and MOCVD.

We also investigated the tunable bandgap and the lattice strain

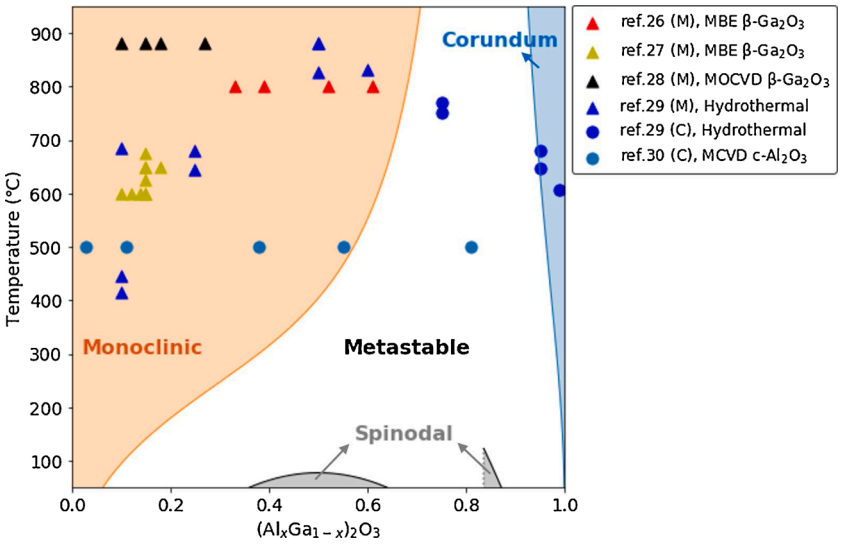

Fig. 4. The calculated phase diagram of $(Al_xGa_{1-x})_2O_3$ alloy system with marked experimental values. The regions shaded with orange and light blue represent stable states of alloy in the monoclinic and corundum structures, respectively. Above and below the black line are metastable and unstable states. The triangle and circle markers represent the experimentally reported structures of monoclinic (M) [26–29] and corundum (C) [29,30], respectively. The experimental data points were obtained by X-ray diffraction methods. The growth method and the substrate used are provided in the legend.

during the alloying process for the application as Ga_2O_3-based electronic devices. The bandgap of the alloy as a function of the molar concentration is given by:

$$E_g(x) = (1-x)E_g[Ga_2O_3] + xE_g[Al_2O_3] - bx(1-x) \quad (5)$$

where $E_g[Ga_2O_3]$ and $E_g[Al_2O_3]$ are the bandgaps of the endpoints in Table I, and b is the bowing parameter. We sampled points for x as analogous to Ω and calculated the b by fitting the bandgap with a single-parabolic equation eq. (5). The evaluated bowing parameter b is shown in Table II. Based on the calculated bandgap of the alloys, we evaluated the[2] correlation between the bandgap and the lattice constant that was a-axis lattice vector in $(Al_xGa_{1-x})_2O_3$ alloy system. In Fig. 5, the bandgaps and lattice constants of Ga_2O_3 linearly increased and decreased by alloying Al, respectively. The bandgap range of $(Al_xGa_{1-x})_2O_3$ alloy system in both structures was 4.52–8.78 eV within a lattice strain of ± 4.38%. We find that the heterostructural alloy is capable of tuning a bandgap more extensive than an $(Al_xGa_{1-x})_2N_3$ [42] system with the isostructural alloy. As stated, we find that the $(Al_xGa_{1-x})_2O_3$ alloy system has attractive properties that can be tuned over a wide range as semiconductor devices. It should be noted that the lattice constant shrinkage strained by the alloying process is inevitable; even if the alloy is grown on a high-quality substrate, the phase separation may occur due to the lattice mismatch. Therefore, stabilizing the heterostructural $(Al_xGa_{1-x})_2O_3$ alloy with good quality is challenging, and further studies are needed for successful phase control.

In addition to the bandgap, the valence- and conduction-band positions of materials are also essential for the design of semiconductor heterostructures [20–22,25–28,30]. We calculated the band energy of disordered $(Al_xGa_{1-x})_2O_3$ alloy against the vacuum level using the electrostatic potential of non-polar monoclinic- (010) and corundum-structure (110) surfaces with the macroscopic electrostatic potential averaging technique [43], as shown in Fig. 6. For both structures, the valence-band maximum (VBM) and the conduction-band minimum (CBM) positions were shown to rises as the molar concentration of Al increases. Using this energy level offset, an enhanced charge density was observed in the modulation-doped field effect transistor (MODFET) [21]. The band offset caused by alloying Al to Ga_2O_3 will be required to overcome the physical limitations of Ga_2O_3-based devices.

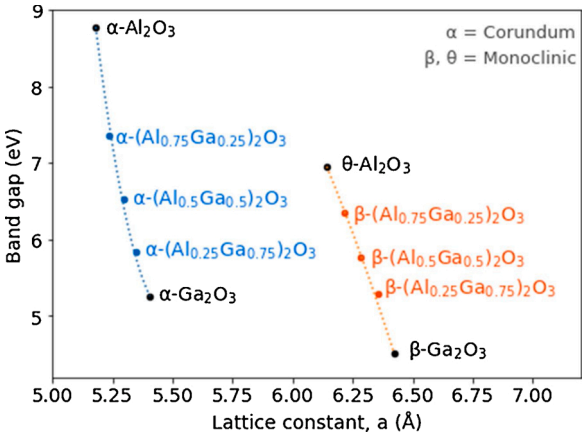

Fig. 5. The correlation between the lattice constant and bandgap of Ga_2O_3 alloyed with Al in the corundum and monoclinic structures. The lattice constants are the a-axis lattice vector of the primitive cell.

4. Conclusion

We investigated the alloying properties of disordered Ga_2O_3-Al_2O_3 systems in both the corundum and monoclinic structures, enthalpy and gibbs free energy. In the monoclinic structure of the alloy, the enthalpy of mixing was low for the molar concentration of Al smaller than 84%, with the possibility to sufficiently overcome ordered alloys by the entropy contribution. The Gibbs-free energy of mixing in both structures was negative at 500 ℃, which is a typical growth temperature. We also identified the stable phase region of $(Al_xGa_{1-x})_2O_3$ alloy in the phase diagram with metastability, which is wider than GaN-AlN alloy systems. This means that alloying Al to Ga_2O_3 is more challenging and sensitive to the process condition. Instead, we show that the bandgap and lattice constant of $(Al_xGa_{1-x})_2O_3$ alloys can be broadly tuned due to its heterostructural nature, which opens a pathway to design novel architecture for electronic devices. The successful phase control of the heterostructural alloy in $(Al_xGa_{1-x})_2O_3$ system will open a new pathway for high-power and high- frequency power electronics.

Declaration of Competing Interest

The authors reported no declarations of interest.

[2] Again, unexpected end of paragraph.
[3] Please remove the indentation.

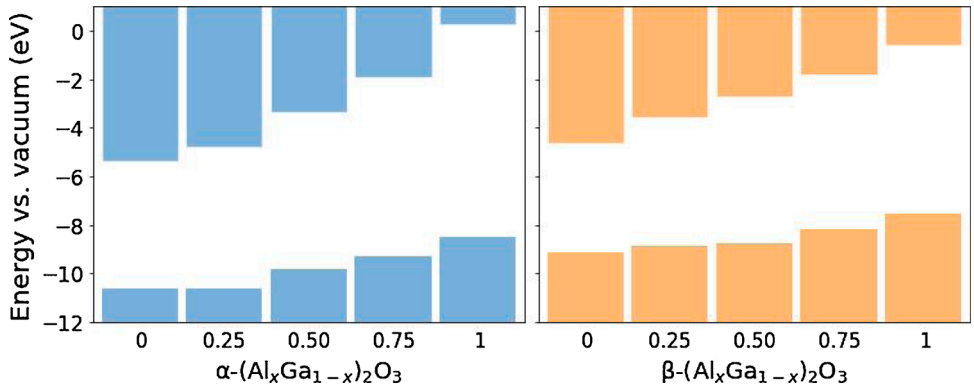

Fig. 6. The calculated valence- and conduction-band positions of α- and β-$(Al_xGa_{1-x})_2O_3$ alloy systems.

Acknowledgments

We gratefully acknowledge partial support from the National Research Foundation of Korea (NRF-2019R1A2B5B01070215 and 2019R1F1A1058554) and Ministry of Trade, Industry & Energy (20004367). The computations were carried out using resources from Korea Supercomputing Center (KSC-2020-CRE-0023).

References

[1] M.A. Mastro, A. Kuramata, J. Calkins, J. Kim, F. Ren, S.J. Pearton, Perspective—opportunities and future directions for Ga_2O_3, ECS J. Solid State Sci. Technol. 6 (5) (2017) P356–P359.
[2] M. Higashiwaki, K. Sasaki, H. Murakami, Y. Kumagai, A. Koukitu, A. Kuramata, T. Masui, S. Yamakoshi, Recent progress in Ga_2O_3 power devices, Semicond. Sci. Technol. 31 (3) (2016), 034001.
[3] M. Higashiwaki, K. Sasaki, A. Kuramata, T. Masui, S. Yamakoshi, Gallium oxide (Ga_2O_3) metal-semiconductor field-effect transistors on single-crystal β-Ga_2O_3 (010) substrates, Appl. Phys. Lett. 100 (1) (2012), 013504.
[4] A.J. Green, K.D. Chabak, E.R. Heller, R.C. Fitch, M. Baldini, A. Fiedler, K. Irmscher, G. Wagner, Z. Galazka, S.E. Tetlak, A. Crespo, K. Leedy, G.H. Jessen, 3.8-MV/cm Breakdown Strength of MOVPE-Grown Sn-Doped β-Ga_2O_3 MOSFETs, IEEE Electron Device Lett. 37 (7) (2016) 902–905.
[5] J.Y. Tsao, S. Chowdhury, M.A. Hollis, D. Jena, N.M. Johnson, K.A. Jones, R. J. Kaplar, S. Rajan, C.G. Van de Walle, E. Bellotti, C.L. Chua, R. Collazo, M. E. Coltrin, J.A. Cooper, K.R. Evans, S. Graham, T.A. Grotjohn, E.R. Heller, M. Higashiwaki, M.S. Islam, P.W. Juodawlkis, M.A. Khan, A.D. Koehler, J.H. Leach, U.K. Mishra, R.J. Nemanich, R.C.N. Pilawa-Podgurski, J.B. Shealy, Z. Sitar, M. J. Tadjer, A.F. Witulski, M. Wraback, J.A. Simmons, Ultrawide-Bandgap Semiconductors: Research Opportunities and Challenges, Adv. Electron. Mater. 4 (1) (2018), 1600501.
[6] J. Park, S.-M. Hong, Simulation Study of Enhancement Mode Multi-Gate Vertical Gallium Oxide MOSFETs, ECS J. Solid State Sci. Technol. 8 (7) (2019) Q3116–Q3121.
[7] J.K. Mun, K. Cho, W. Chang, H.-W. Jung, J. Do, Editors' choice—2.32 kV Breakdown Voltage Lateral β-Ga_2O_3 MOSFETs with Source-Connected Field Plate, ECS J. Solid State Sci. Technol. 8 (7) (2019) Q3079–Q3082.
[8] S. Yoshioka, H. Hayashi, A. Kuwabara, F. Oba, K. Matsunaga, I. Tanaka, Structures and energetics of Ga_2O_3 polymorphs, J. Phys. Condens. Matter 19 (34) (2007), 346211.
[9] R. Roy, V.G. Hill, E.F. Osborn, Polymorphism of Ga_2O_3 and the system Ga_2O_3—H2O, J. Am. Chem. Soc. 74 (3) (1952) 719–722.
[10] V.D. Wheeler, N. Nepal, D.R. Boris, S.B. Qadri, L.O. Nyakiti, A. Lang, A. Koehler, G. Foster, S.G. Walton, C.R. Eddy, D.J. Meyer, Phase Control of Crystalline Ga_2O_3 Films by Plasma-Enhanced Atomic Layer Deposition, Chem. Mater. 32 (3) (2020) 1140–1152.
[11] H. Aida, K. Nishiguchi, H. Takeda, N. Aota, K. Sunakawa, Y. Yaguchi, Growth of β-Ga_2O_3 Single Crystals by the Edge-Defined, Film Fed Growth Method, Jpn. J. Appl. Phys. 47 (11) (2008) 8506–8509.
[12] Z. Galazka, K. Irmscher, R. Uecker, R. Bertram, M. Pietsch, A. Kwasniewski, M. Naumann, T. Schulz, R. Schewski, D. Klimm, M. Bickermann, On the bulk β-Ga_2O_3 single crystals grown by the Czochralski method, J. Cryst. Growth 404 (2014) 184–191.
[13] D.-W. Jeon, H. Son, J. Hwang, A.Y. Polyakov, N.B. Smirnov, I.V. Shchemerov, A. V. Chernykh, A.I. Kochkova, S.J. Pearton, I.-H. Lee, Electrical properties, structural properties, and deep trap spectra of thin α-Ga_2O_3 films grown by halide vapor phase epitaxy on basal plane sapphire substrates, APL Mater. 6 (12) (2018), 121110.
[14] R. Schewski, G. Wagner, M. Baldini, D. Gogova, Z. Galazka, T. Schulz, T. Remmele, T. Markurt, H. von Wenckstern, M. Grundmann, O. Bierwagen, P. Vogt, M. Albrecht, Epitaxial stabilization of pseudomorphic α-Ga_2O_3 on sapphire (0001), Appl. Phys. Express 8 (1) (2014), 011101.
[15] F. Mezzadri, G. Calestani, F. Boschi, D. Delmonte, M. Bosi, R. Fornari, Crystal Structure and Ferroelectric Properties of ε-Ga_2O_3 films grown on (0001)-Sapphire, lnorg. Chem. 55 (22) (2016) 12079–12084.
[16] S.B. Cho, R. Mishra, Epitaxial engineering of polar ε-Ga_2O_3 for tunable two-dimensional electron gas at the heterointerface, Appl. Phys. Lett. 112 (16) (2018), 162101.
[17] S. Luan, L. Dong, X. Ma, R. Jia, The further investigation of N-doped β-Ga_2O_3 thin films with native defects for Schottky-barrier diode, J. Alloys Compd. 812 (2020), 152026.
[18] H. Peelaers, J.B. Varley, J.S. Speck, C.G. Van de Walle, Structural and electronic properties of Ga_2O_3-Al_2O_3 alloys, Appl. Phys. Lett. 112 (24) (2018), 242101.
[19] T. Wang, W. li, C. Ni, A. Janotti, Band gap and Band Offset of Ga_2O_3 and $(Al_xGa_{1-x})_2O_3$ alloys, Phys. Rev. Appl. 10 (2018), 011003.
[20] T. Oshima, Y. Kato, N. Kawano, A. Kuramata, S. Yamakoshi, S. Fujita, T. Oishi, M. Kasu, Carrier confinement observed at modulation-doped β-$(Al_xGa_{1-x})_2O_3$/Ga_2O_3 heterojunction interface, Appl. Phys. Express 10 (3) (2017), 035701.
[21] S. Krishnamoorthy, Z. Xia, C. Joishi, Y. Zhang, J. McGlone, J. Johnson, M. Brenner, A.R. Arehart, J. Hwang, S. Lodha, S. Rajan, Modulation-doped β-$(Al_{0.2}Ga_{0.8})_2O_3$/Ga_2O_3 field-effect transistor, Appl. Phys. Lett. 111 (2) (2017), 023502.
[22] E. Ahmadi, O.S. Koksaldi, X. Zheng, T. Mates, Y. Oshima, U.K. Mishra, J.S. Speck, Demonstration of β-$(Al_xGa_{1-x})_2O_3$/β-Ga_2O_3 modulation doped field-effect transistors with Ge as dopant grown via plasma-assisted molecular beam epitaxy, Appl. Phys. Express 10 (7) (2017), 071101.
[23] S.J. Pearton, J. Yang, P.H. CaryIV, F. Ren, J. Kim, M.J. Tadjer, M.A. Mastro, A review of Ga_2O_3 materials, processing, and devices, Appl. Phys. Rev. 5 (1) (2018), 011301.
[24] H. Zhang, L. Yuan, X. Tang, J. Hu, J. Sun, Y. Zhang, Y. Zhang, R. Jia, Progress of Ultra-Wide Bandgap Ga_2O_3 Semiconductor Materials in Power MOSFETs, IEEE Trans. Power Electron. 35 (5) (2020) 5157–5179.
[25] E. Ahmadi, Y. Oshima, F. Wu, J.S. Speck, Schottky barrier height of Ni to β-$(Al_xGa_{1-x})_2O_3$ with different compositions grown by plasma-assisted molecular beam epitaxy, Semicond. Sci. Technol. 32 (3) (2017), 035004.
[26] T. Oshima, T. Okuno, N. Arai, Y. Kobayashi, S. Fujita, β-$Al_{2x}Ga_{2-2x}O_3$ Thin Film Growth by Molecular Beam Epitaxy, Jpn. J. Appl. Phys. 48 (7) (2009), 070202.
[27] S.W. Kaun, F. Wu, J.S. Speck, β-$(Al_xGa_{1-x})_2O_3$/Ga_2O_3 (010) heterostructures grown on β- Ga_2O_3 (010) substrates by plasma-assisted molecular beam epitaxy, J. Vac. Sci. Technol. 33 (4) (2015), 041508.
[28] A.F.M.A.U. Bhuiyan, Z. Feng, J.M. Johnson, Z. Chen, H.-L. Huang, J. Hwang, H. Zhao, MOCVD epitaxy of β-$(Al_xGa_{1-x})_2O_3$ thin films on (010) Ga_2O_3 substrates and N-type doping, Appl. Phys. Lett. 115 (12) (2019), 120602.
[29] V.G. Hill, R. Roy, E.F. Osborn, The System Alumina-Gallia-Water, J. Am. Ceram. Soc. 35 (6) (1952) 135–142.
[30] H. Ito, K. Kaneko, S. Fujita, Growth and Band Gap Control of Corundum-Structured α-$(AlGa)_2O_3$ Thin Films on Sapphire by Spray-Assisted Mist Chemical Vapor Deposition, Jpn. J. Appl. Phys. 51 (2012), 100207.
[31] A.M. Holder, S. Siol, P.F. Ndione, H. Peng, A.M. Deml, B.E. Matthews, L. T. Schelhas, M.F. Toney, R.G. Gordon, W. Tumas, J.D. Perkins, D.S. Ginley, B. P. Gorman, J. Tate, A. Zakutayev, S. Lany, Novel phase diagram behavior and materials design in heterostructural semiconductor alloys, Sci. Adv. 3 (6) (2017), e1700270.
[32] G. Kresse, J. Furthmüller, Efficient iterative schemes for ab initio total-energy calculations using a plane-wave basis set, Phys. Rev. B 54 (16) (1996) 11169–11186.
[33] P.E. Blöchl, Projector augmented-wave method, Phys. Rev. B 50 (24) (1994) 17953–17979.
[34] J.P. Perdew, K. Burke, M. Ernzerhof, Generalized Gradient Approximation Made Simple, Phys. Rev. Lett. 77 (18) (1996) 3865–3868.
[35] J. Heyd, G.E. Scuseria, M. Ernzerhof, Hybrid functionals based on a screened Coulomb potential, J. Chem. Phys. 118 (18) (2003) 8207–8215.
[36] R.H. French, Electronic band structure of Al_2O_3, with comparison to Alon and AIN, J. Am. Ceram. Soc. 73 (3) (1990) 477–489.

[37] T. Matsumoto, M. Aoki, A. Kinoshita, T. Aono, Absorption and Reflection of Vapor Grown Single Crystal Platelets of β-Ga_2O_3, Jpn. J. Appl. Phys. 13 (10) (1974) 1578–1582.
[38] A. Zunger, S.H. Wei, L.G. Ferreira, J.E. Bernard, Special quasirandom structures, Phys. Rev. Lett. 65 (3) (1990) 353–356.
[39] A. van de Walle, P. Tiwary, M. de Jong, D.L. Olmsted, M. Asta, A. Dick, D. Shin, Y. Wang, L.Q. Chen, Z.K. Liu, Efficient stochastic generation of special quasirandom structures, Calphad 42 (2013) 13–18.
[40] Ih. Ho, G.B. Stringfellow, Solid phase immiscibility in GaInN, Appl. Phys. Lett. 69 (18) (1996) 2701–2703.
[41] H. Peng, P. Ndione, D. Ginley, A. Zakutayev, S. Lany, Design of Semiconducting Tetrahedral Mn 1 − x Zn x O Alloys and Their Application to Solar Water Splitting, Phys. Rev. X 5 (2015), 021016.
[42] R.R. Pelá, C. Caetano, M. Marques, L.G. Ferreira, J. Furthmüller, L.K. Teles, Accurate band gaps of AlGaN, InGaN, and AlInN alloys calculations based on LDA-1/2 approach, Appl. Phys. Lett. 98 (15) (2011), 151907.
[43] V. Stevanović, S. Lany, D.S. Ginley, W. Tumas, A. Zunger, Assessing capability of semiconductors to split water using ionization potentials and electron affinities only, Phys. Chem. Chem. Phys. 16 (8) (2014) 3706–3714.